INORGANIC CHEMISTRY

FRONTIERS

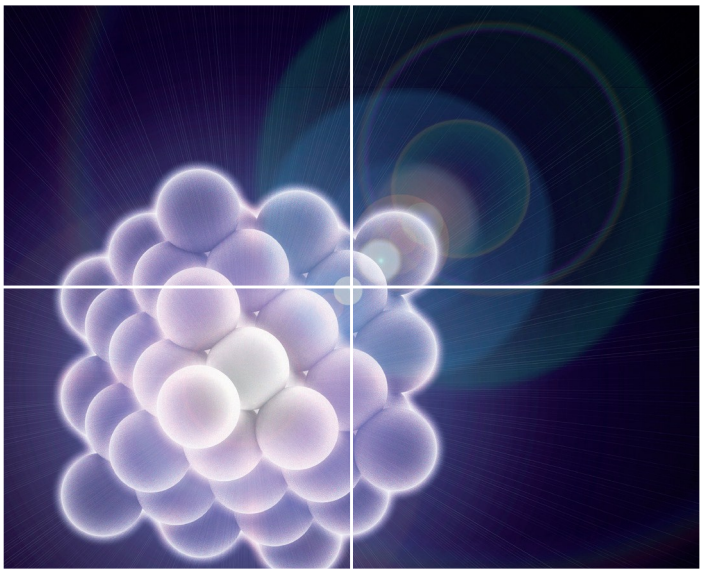

Accepted Manuscript

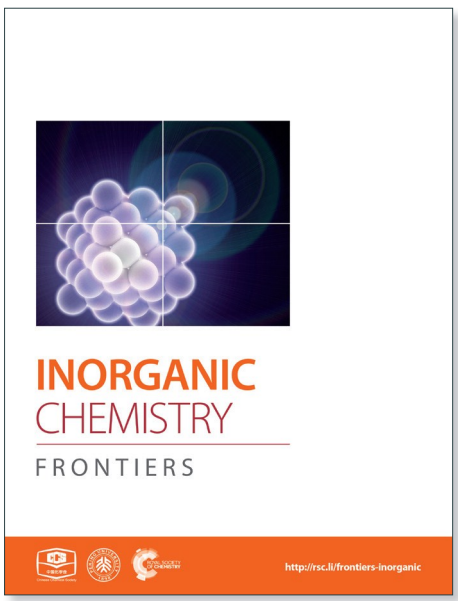

This is an *Accepted Manuscript*, which has been through the Royal Society of Chemistry peer review process and has been accepted for publication.

Accepted Manuscripts are published online shortly after acceptance, before technical editing, formatting and proof reading. Using this free service, authors can make their results available to the community, in citable form, before we publish the edited article. We will replace this *Accepted Manuscript* with the edited and formatted *Advance Article* as soon as it is available.

You can find more information about *Accepted Manuscripts* in the **Information for Authors**.

Please note that technical editing may introduce minor changes to the text and/or graphics, which may alter content. The journal's standard **Terms & Conditions** and the **Ethical guidelines** still apply. In no event shall the Royal Society of Chemistry be held responsible for any errors or omissions in this *Accepted Manuscript* or any consequences arising from the use of any information it contains.

DFT and TD-DFT studies of electronic structures and one-electron excitation state of cyanide-bridged molecular square complex

Yasutaka Kitagawa*[1)], Mizuki Asaoka[1)], Koji Miyagi[1)], Toru Matsui[2)], Masayuki Nihei[3)], Hiroshi Oshio[3)], Mitsutaka Okumura[2)], Masayoshi Nakano[1)]

1) Graduate School of Engineering Science, Science, Osaka University, 1-3 Machikaneyama, Toyonaka, Osaka 560-8531, Japan,
2) Graduate School of Science, Osaka University, 1-1 Machikaneyama, Toyonaka, Osaka 560-0043, Japan,
3) Graduate School of Pure and Applied Sciences, University of Tsukuba, Tennodai 1-1-1, Tsukuba, Ibaraki 305-8571, Japan.

Abstract

Electronic structures of a cyanide bridged Fe-Co molecular square, $[Co_2Fe_2(CN)_6(tp^*)_2(dtbbpy)_4](PF_6)_2 \cdot 2MeOH$ (**1**) (tp* = hydrotris (3,5-dimethylpyrazol-1-yl) borate, dtbbpy =4,4'-di-*tert*-butyl-2,2'-bipyridine), which exhibits thermal and photo-induced two-step charge-transfer induced spin transitions (CTIST), are investigated in detail by density functional theory (DFT) and time-dependent (TD) DFT calculations. For three phases observed by the experiment, three different model structures are constructed based on the geometries of X-ray crystallography analyses measured at low (100K), middle (298K) and high (330K) temperatures. Calculated results elucidate that the ground states at the low and the high temperatures are diamagnetic $[(Fe^{II}_{LS})_2(Co^{III}_{LS})_2]$ and ferromagnetic $[(Fe^{III}_{LS})_2(Co^{II}_{HS})_2]$ states, respectively. On the other hand, the one-electron transferred $[Fe^{II}_{LS}Fe^{III}_{LS}Co^{II}_{HS}Co^{III}_{LS}]$ state becomes the ground state at the intermediate temperature phase. A magnetic interaction between Fe^{III} and Co^{II} in the $[(Fe^{III}_{LS})_2(Co^{II}_{HS})_2]$ state is ferromagnetic and the most stable spin-coupling state is the all-ferromagnetic state. The TD-DFT calculation shows the two significant peaks about Fe^{II} $t_{2g} \rightarrow Co^{III}$ e_g around 800nm. The result supports that the experimental broad absorption peak at 770 nm is an inter-valence charge transfer (IVCT) band.

*Corresponding author: Yasutaka Kitagawa,
E-mail: kitagawa@cheng.es.osaka-u.ac.jp

1. Introduction

Prussian blue that is formally written $Fe_4[Fe(CN)_6]_3 \cdot xH_2O$ is one of the well-known dyes. The iron ions in the compound can be easily substituted by other metal ions such as Cr, Mn, Co and so on, and those are called Prussian blue analogues (PBAs). The PBAs are 3D bulk materials that metal ions are bridged by cyanide ions. The cyanide ions mediate electronic and magnetic interactions between metal ions, therefore intriguing physical properties are found in the PBAs, such as high critical temperature (*T*c) magnets, spin-crossover, linkage isomerism, and ferro-electricity.[1-11] One of the most important physical properties of the PBAs is a ferromagnetism. Babel et al. first found the ferromagnetism in $Cs^{I}Mn^{II}[Cr^{III}(CN)_6] \cdot H_2O$ (*T*c=90K).[1] About a decade later, Verdaguer and co-workers also found that $Cs(I)Ni(II)[Cr(III)(CN)_6] \cdot 2H_2O$ showed the ferromagnetism (*T*c=90K).[2] His group has contributed to increase the *T*c of those systems, and has finally found a high *T*c ferromagnet; $V^{II}_{0.42}V^{III}_{0.58}[Cr^{III}(CN)_6]_{0.86} \cdot 2.8H_2O$ (*T*c=315K).[3] In addition, Sato et al. has revealed that a magnetic property of $K_{0.2}Co_{1.4}[Fe(CN)_6] \cdot 6.9H_2O$ is changed from paramagnetic to ferrimagnetic by the irradiation of a 450nm light, suggesting that a long-range magnetic order can be controlled by external stimuli.[5] The photo-irradiation to those systems often causes the inter valence charge transfer (IVCT), and it sometimes changes the spin structure, which is called as a charge transfer induced spin transition (CTIST).[6] Those phenomena, as well as the light induced spin transition and the light induced excited spin state trapping (LIESST), are sometimes utilized for the optical switching.[7] Therefore, the PBAs have attracted a wide attention from both fundamental science and applied materials.[8,9] On the other hand, cuban- or square-type of hexacyanide complexes can be regareded as a part of the PBA compounds. Because of such distinguished magnetic properties, those complexes have been considerd to be a promissing candidate for the molecular magnets.[10] There has been many reports about single molecular magnet (SMM) and related complexes in this two decades.[6,11-13]

In 2010, Oshio and co-workers have reported that a PBA-type cyanide-bridged molecular square complex; $[Co_2Fe_2(CN)_6(tp^*)_2(dtbbpy)_4](PF_6)_2 \cdot 2MeOH$ (**1**) （pt* = hydrotris(3,5-dimethylpyrazol-1- yl)borate, dtbbpy = 4,4'-di-*tert*-butyl-2,2'-bipyridine）shows CTIST by thermal and photo excitations.[6] The complex shows thermochromism from a dark red at 330K to dark green at 250K.

Magnetic susceptibility measurements elucidate that the complex **1** is diamagnetic at a low temperature (LT) phase (~250K). However $\chi_m T$ value becomes 6.57 emu mol^{-1} K at a high temperature (HT) phase (330K), suggesting that the complex consists of low-spin (LS) Fe^{III} (s=1/2) and high-spin (HS) Co^{II} (s=3/2). At an intermediate region between LT and HT phases (275~310K), there is a step in $\chi_m T$ values, indicating an existence of the intermediate phase as illustrated in Figure S1 in Supplementary materials. The X-ray crystallographic analyses at 100, 298 and 330K reveal that the complex is a square structure consists of Fe and Co ions. The both magnetic and structural results suggest $[(Fe^{II}_{LS})_2(Co^{III}_{LS})_2]$ and $[(Fe^{III}_{LS})_2(Co^{II}_{HS})_2]$ for the LT and HT phases, respectively. On the other hand, at the intermediate phase, there are still two possibilities of the electronic structure; *i.e.* one-electron transferred $[Fe^{II}_{LS}Fe^{III}_{LS}Co^{II}_{HS}Co^{III}_{LS}]$ state or a 1:1 mixture of $[(Fe^{III}_{LS})_2(Co^{II}_{HS})_2]$ and $[(Fe^{II}_{LS})_2(Co^{III}_{LS})_2]$. At the LS phase, the complex has a broad absorption peak around 770nm that is considered to be the $Fe^{II}\rightarrow Co^{III}$ IVCT band. Significantly, an 808 nm laser irradiation to the complex **1** in the LT phase causes a rapid increase of $\chi_m T$ values. The result suggests that the light-induced CTIST is occurred in the LT phase. Although such physical properties have been reported, details about electronic structures at each temperature, and a relation between electronic structures and properties have not been elucidated sufficiently.

On the other hand, a recent progress of computers and density functional theory (DFT) realizes the first principal calculations of electronic structures for real large molecules, so that a direct estimation of the physical properties becomes feasible. In addition, there have been advances in a computational scheme to obtain the J values of diradical or polyradical species to explain the magnetic behaviors.[14-16] In this sense, the DFT method is a powerful tool for the analyses of the electronic structures and physical properties of the complex **1**. Up to now, there have been several reports about theoretical calculations about PBAs especially for magnetic properties, however the computational models are still insufficient to consider the properties of whole molecules.[14]

For the above reasons, in this paper, we perform DFT calculations to elucidate the detail about the electronic structures and the relation between electronic structures and magnetic properties of the complex **1**, with sufficient model structures including all

metal ions. The electronic and spin structures are calculated at low, middle and high temperature structures, and the *J* values between metal ions are obtained for the high temperature structure. In addition, the one-electron excitation state of the complex **1** is also examined to verify the $Fe^{II} \rightarrow Co^{III}$ IVCT at the low temperature structure.

2. Computational details

2. 1 Construction of model structures and calculated charge and spin states

Based on the coordinate of the complex **1** measured by X-ray crystallography analyses, model structures for the DFT calculations are constructed. In order to consider a structural change with temperatures, molecular geometries are taken from the data measured at three different temperatures that correspond to low, intermediate and high temperature phases, namely 100K, 298K and 330K.[17] A contribution of the substitution groups of the ligands is also examined by using full and reduced model structures. The full model consists of a whole structure of the complex **1**, except for counter ions and MeOH in the crystal as illustrated in Figure 1 (a). On the other hand, in the case of the reduced model structure, *tert*-butyl and methyl groups of dtbbpy and tp* ligands are substituted for hydrogen atoms as shown in the Figure 1(b). The model structures of the complex **1** in low (100K), middle (intermediate) (298K) and high (330K) temperature phases are defined as **1-L**, **1-M** and **1-H**, respectively, and their important structural parameters are summarized in Figure 1 (c). Unless otherwise noted, those abbreviations indicate the reduced models, and the full model is specified in the text.

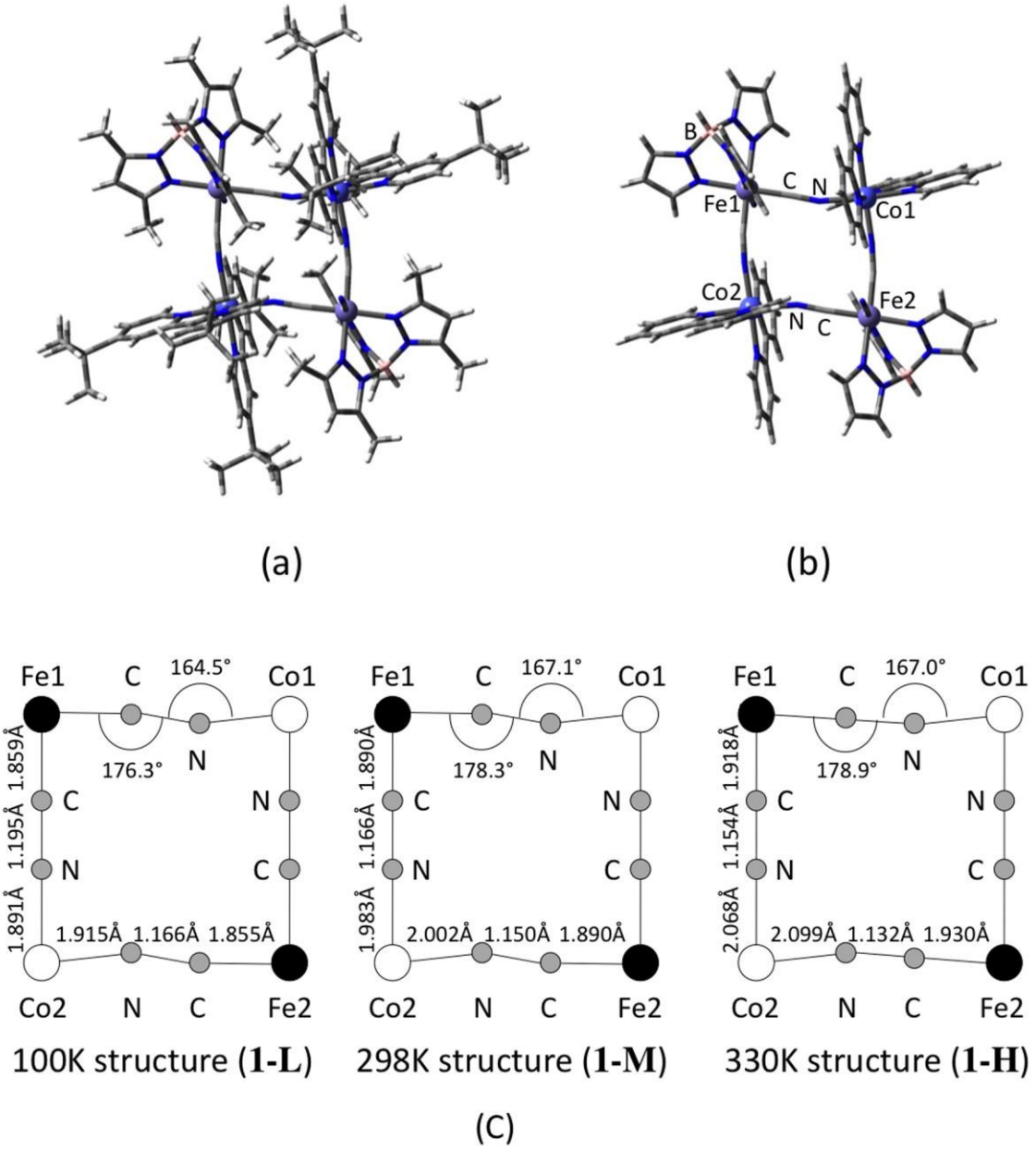

Figure 1 Calculated model structures of complex **1**. (a) Full model and (b) reduced model structures. (c) Structural parameters measured at different temperatures

In addition to the geometric differences with the temperature, we examined two types of charge and spin states, namely $[(Fe^{II}_{LS})_2(Co^{III}_{LS})_2]$ and $[(Fe^{III}_{LS})_2(Co^{II}_{HS})_2]$ states, for each temperature model structure. And $[Fe^{II}_{LS}Fe^{III}_{LS}Co^{II}_{HS}Co^{III}_{LS}]$ state is also calculated especially for the **1-M** model structure. Because $[(Fe^{III}_{LS})_2(Co^{II}_{HS})_2]$ and $[Fe^{II}_{LS}Fe^{III}_{LS}Co^{II}_{HS}Co^{III}_{LS}]$ states have open-shell spin structures that contain Fe^{III}_{LS}

(s=1/2) and Co^{II}_{HS} (s=3/2) ions, both spin-coupling structures of ferromagnetic and anti-ferromagnetic states are obtained as explained below. Note that the word "anti-ferromagnetic" used here must be denoted by "ferri-magnetic", however we use the expression to focus on the locally adjacent interaction. The $[(Fe^{III}_{LS})_2(Co^{II}_{HS})_2]$ state possesses three intra-molecular magnetic interaction (J, J' and J'') as illustrated in Figure 2 (a). Consequently there are five possible spin-coupling states as illustrated in Figure S2 in Supplementary materials. Here we examine two of them as illustrated in Figure 2 (b) and (c). The spin-coupling state in Figure 2 (b) is that all adjacent spin-spin interactions are ferromagnetic (S_Z=4), while the state in Figure 2 (c) is anti-ferromagnetic (S_Z=2). Information about those spin-coupling structures (diamagnetic (D), ferromagnetic (F) or anti-ferromagnetic (AF)) is added to the abbreviations of the model structures by subscripts (see Table 1). The spin-coupling states between Fe^{III}_{LS} and Co^{II}_{HS} in $[Fe^{II}_{LS}Fe^{III}_{LS}Co^{II}_{HS}Co^{III}_{LS}]$ state, which has a single intra-molecular magnetic interaction, are also defined as partial ferromagnetic (PF) (S_Z=2) and partial anti-ferromagnetic (PAF) (S_Z=1) interactions here. From these points of view, we carried out totally 12 single-point calculations as summarized in Table 1.

Table 1. Classifications and abbreviations of calculated models by structures, charge and spin states.

Model size	Charge state	Spin state and magnetic interaction	Temperature of X-ray crystallography		
			100K	298K	330K
Full	$[(Fe^{II}_{LS})_2(Co^{III}_{LS})_2]$	Diamagnetic (D)	**Full-1-L_D**	–	–
Reduced[a)]	$[(Fe^{II}_{LS})_2(Co^{III}_{LS})_2]$	Diamagnetic (D)	**1-L_D**	**1-M_D**	**1-H_D**
	$[(Fe^{III}_{LS})_2(Co^{II}_{HS})_2]$	Ferromagnetic (F)	**1-L_F**	**1-M_F**	**1-H_F**
		Anti-Ferromagnetic (AF)	**1-L_{AF}**	**1-M_{AF}**	**1-H_{AF}**
	$[Fe^{II}_{LS}Fe^{III}_{LS}Co^{II}_{HS}Co^{III}_{LS}]$	Partial Ferromagnetic (PF)	–	**1-M_{PF}**	–
		Partial Anti-ferromagnetic (PAF)	–	**1-M_{PAF}**	–

a) An abbreviation meaning "the reduced model" is omitted here.

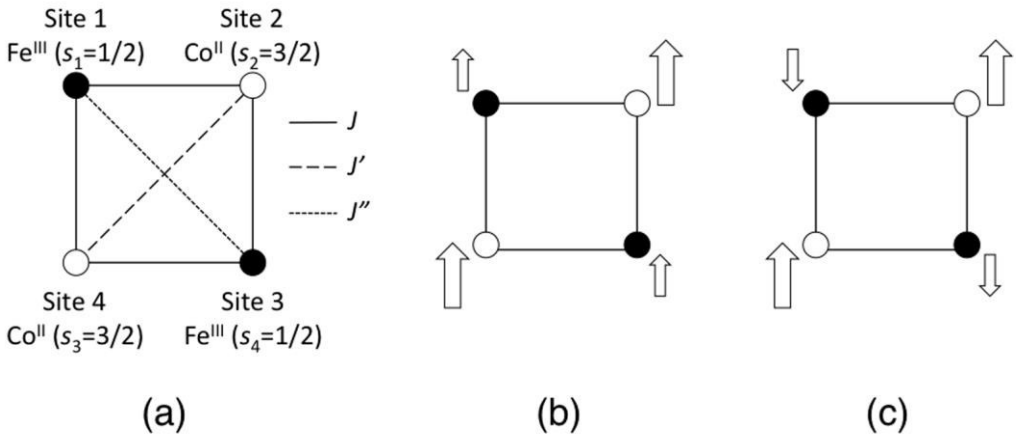

Figure 2 (a) Illustrations of magnetic interactions between spin sites in the open-shell $[(Fe^{III}_{LS})_2(Co^{II}_{HS})_2]$ state. (b) The ferromagnetic (F) state. (c) The anti-ferromagnetic (AF) state. A size of arrow expresses a size of spin magnitude at each spin site.

2.2 Functional sets and basis sets

The electronic structures of those structural models and charge-spin states are calculated by the use of a hybrid DFT of the Becke-3-Lee-Yang-Parr (B3LYP) functional set on Gaussian 09.[18] The basis functions used for all calculations are Huzinaga MIDI plus p-type orbitals for Fe and Co ions, 6-31+G* for cyanide ligands and 6-31G* for other atoms. For the diamagnetic state that consists of the low spin Fe^{II} and Co^{III} ions, a spin-restricted (R) calculation is applied. On the other hand, for the open-shell (F, AF, PF and PAF) states that consist of Fe^{III} and Co^{II} ions, the broken-symmetry (BS) calculation is employed to approximate the static correlation by the quasi-degenerate orbitals and to express localized spins on each metal site.[19] We also carry out a time-dependent (TD) B3LYP calculation on **1-L$_D$** with the same functional set and basis sets to elucidate orbitals concerning the IVCT that is the electron excitation from Fe^{II} to Co^{III} at the low temperature diamagnetic state. The environmental condition is assumed to be in the gas phase due to the computational costs.

3. Calculated results

*3.1 Electronic structure of the complex **1** in the low temperature phase*

The electronic structure of the complex **1** at the low temperature phase is examined by the model structures **1-L$_X$** (X = D, F, AF). As a first step, molecular orbitals (MOs) of the full model (**Full-1-L$_D$**) are compared with those of the reduced model (**1-L$_D$**) to elucidate an influence of the *tert*-butyl and methyl groups of the dtbbpy and the tp* ligands upon the electronic structure. The calculated MOs around the highest occupied MO (HOMO) and the lowest unoccupied MO (LUMO) of them are depicted in Figure 3. All valence electron orbitals are doubly quasi-degenerated reflecting C_2 symmetry of the complex. Orbital shapes of **Full-1-L$_D$** and **1-L$_D$** depicted in the figure are quite similar to each other. HOMO – HOMO-2 of both models mainly consist of Fe t_{2g} orbitals that form π-type anti-bonding orbitals with bridging cyanide and tb* ligands. LUMO – LUMO+3 are localized at the dtbbpy ligands, and unoccupied Co e_g orbitals are found in LUMO+4 – LUMO+7. Those Co e_g orbitals are almost localized at Co ions but show weak σ-type anti-bonding interactions with tb* ligands.

Frontier orbital energies of **1-L$_D$** are generally stabilized about 0.7 – 0.8 eV in comparison with those of **Full-1-L$_D$**. However there are not significant differences in orbital energy gaps. For example, the HOMO-LUMO gaps of **Full-1-L$_D$** and **1-L$_D$** are 1.73 and 1.63 eV, respectively. In addition, orbital energy gaps between HOMO (Fe t_{2g}) and unoccupied Co e_g orbitals relating to the IVCT from Fe^{II} to Co^{III} are also 2.01 and 2.08 eV on **Full-1-L$_D$**, **1-L$_D$**, respectively. It suggests that absorption spectrum of **1-L$_D$** simulated by the TD-DFT qualitatively correspond to that of **Full-1-L$_D$**. Those orbital analyses, in summary, indicate that orbital shapes, configurations and orbital energy gaps of the valence electrons of the full model are consistent with those of the reduced model. In other words, the *tert*-butyl and methyl groups of the dtbbpy the tp* ligands do not show a significant effect on the valence electron properties but are expected to contribute to a stability of the molecular structure at each temperature. From this point of view, the reduced mode structure is used for the following all calculations.

With the use of the reduced model, we also calculate the electronic structures of the open-shell $[(Fe^{III}_{LS})_2(Co^{II}_{HS})_2]$ *i.e.* **1-L$_F$** and **1-L$_{AF}$**. Calculated their total and relative energies are summarized in Table 2, together with data on **1-L$_D$**. The most stable state is **1-L$_D$** and the open-shell states are unstable about 2.3 – 2.4 eV. This

result is consistent with the experimental result that the diamagnetic state $[(Fe^{II}_{LS})_2(Co^{III}_{LS})_2]$ is the ground state at the low temperature. On the other hand, the total energy of **1-L$_F$** is slightly lower than that of **1-L$_{AF}$**, indicating that the magnetic interaction between Fe^{III}_{LS} and Co^{II}_{HS} is ferromagnetic as discussed below.

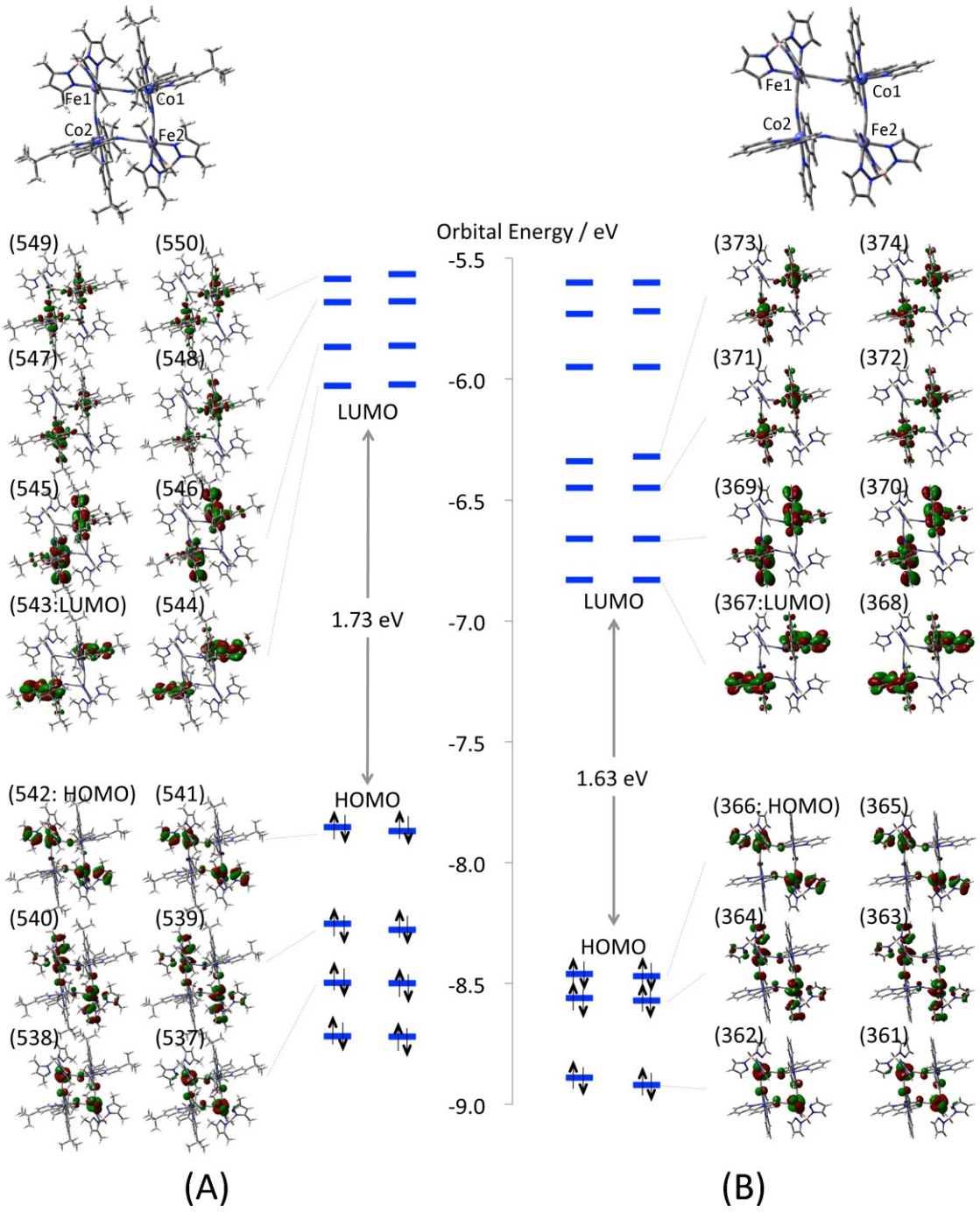

Figure 3. Molecular orbitals of (A) full model (**Full-1-L$_D$**) and (B) reduced model (**1-L$_D$**). Numbers on the MOs indicate orbital numbers. Enlarged MOs are also summarized in supplementary materials (Figure S3).

Table 2. Calculated total and relative energies[a] of **1-L**. $\langle S^2 \rangle$ values are also summarized in parentheses.

Models/States	Total energy / atomic unit	Relative energy / eV
1-L$_D$	-9234.234844 (0.0000)	0.00
1-L$_F$	-9234.149165 (20.0798)	2.33
1-L$_{AF}$	-9234.147959 (8.0608)	2.36

[a] *Relative energy* = $E(\boldsymbol{X}) - E(\mathbf{1\text{-}L_D})$, $\boldsymbol{X}$ = **1-L$_D$**, **1-L$_F$**, **1-L$_{AF}$**

*3.2 Electronic and spin structures of the complex **1** in the high temperature phase*

As a next step, the electronic structure of the complex **1** at the high temperature phase is examined by using the X-ray geometry measured at 330K. From the experimental results, the open-shell [$(Fe^{III}_{LS})_2(Co^{II}_{HS})_2$] state is considered to be the ground state so that we examine two spin-coupling states as illustrated in Figure 2 (b) and (c) on the reduced model structure (**1-H$_X$** (X = F, AF)) by BS-B3LYP. For the comparison, we also examine the D state by R-B3LYP.

First, calculated MOs around HOMO-SOMO-LUMO of the F (Fe^{III} s=1/2; Co^{II} s=3/2) and the AF (Fe^{III} s=–1/2; Co^{II} s=3/2) states are depicted in Figure 4 (a) and (b), respectively. In the case of the F state, both α and β HOMOs that are doubly quasi-degenerate consist of anti-bonding orbitals between tp* ligands (dominant contribution) and Fe^{III} t_{2g} orbitals. The doubly quasi-degenerate β LUMOs that are consisted of Fe^{III} t_{2g} orbitals locate 3.26 eV above the β HOMO. The β LUMO+2 orbital (orbital No. 365 in Figure 4 (a)), which locates 3.92 eV above the β HOMO consists mainly of Co^{II} e_g orbitals. On the other hand, the AF state also has doubly quasi-degenerate HOMOs consist of anti-bonding orbitals between tp* ligands (dominant contribution) and Fe^{III} t_{2g} orbitals. The unoccupied Fe^{III} t_{2g} orbitals of the AF state appear as α LUMOs, and the unoccupied Co e_g orbital is found as a β LUMO.

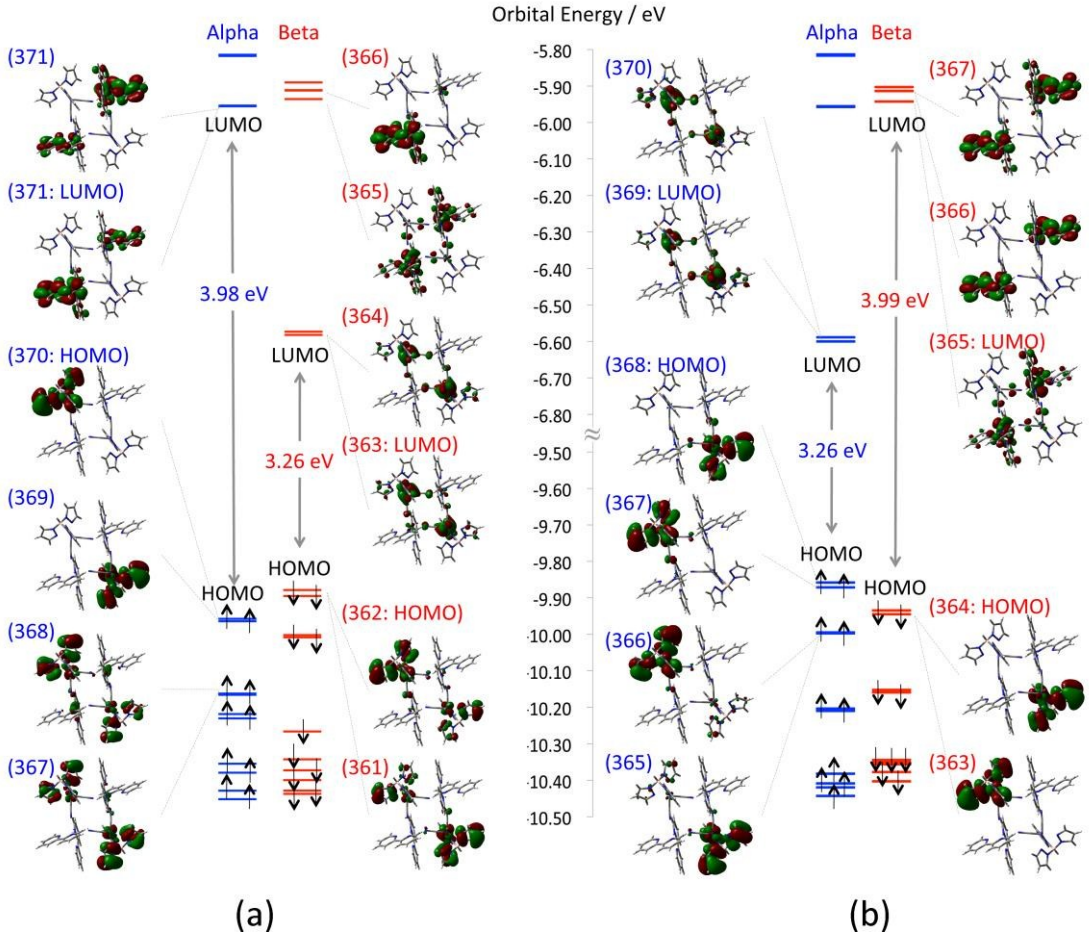

Figure 4. Depicted molecular orbitals of (a) ferromagnetic state (**1-H$_F$**) and (b) anti-ferromagnetic state (**1-H$_{AF}$**). Orbital energy levels of α and β orbitals are marked by blue and red lines, respectively. Numbers on the MOs indicate orbital numbers. Enlarged MOs are also summarized in supplementary materials (Figure S4).

Next, calculated total energies, $\langle S^2 \rangle$ values, and Mulliken spin densities for the F, the AF and the D states are summarized in Table 2. In contrast to the low temperature models, the open-shell states *i.e.* **1-H$_F$** and **1-H$_{AF}$** are stable in comparison with the D state. The energy difference between the most stable **1-H$_F$** and the unstable **1-H$_D$** is about 4 eV that is enlarged in comparison with the low temperature model. Absolute values of spin densities that are 0.95 – 1.0 and 2.7 on Fe and Co ions correspond to the spins of Fe^{III}_{LS} and Co^{II}_{HS}, respectively. And the results also indicate that spins are almost localized on each metal ions. Total energy of **1-H$_F$** is slightly stable than that of **1-H$_{AF}$**, suggesting that the interaction between adjacent Co and Fe

ions is ferromagnetic also in the high temperature model.

Table 3. Calculated total energies, relative energies[a] $\langle S^2 \rangle$ values and Mulliken spin densities by BS-B3LYP for F, AF states and by R-B3LYP for D state of **1-H** model structures.

	Models/States		
	1-H$_F$	**1-H$_{AF}$**	**1-H$_D$**
Energy / atomic unit	-9234.084338	-9234.083755	-9233.936248
(Relative Energy / eV)	(0.00)	(0.02)	(4.03)
$\langle S^2 \rangle$	20.0485	8.0443	0.0000
Mulliken spin densities			
Co (average)	2.70	2.70	0.00
Fe (average)	0.95	-1.00	0.00
C (Bridge)	0.06	0.02	0.00
N (Bridge)	0.01	0.05	0.00

[a] *Relative energy* = $E(\boldsymbol{X}) - E(\mathbf{1\text{-}H_F})$, $\boldsymbol{X}$ = **1-H$_D$**, **1-H$_F$**, **1-H$_{AF}$**

3.3 Possible electronic states in the intermediate phase

The calculated results that the ground states of the complex **1** at the low and high temperature models are the D and the F states, respectively, are consistent with the experiment. However, the electronic structure in the intermediate phase at the middle temperature is still unclear. The two possibilities are suggested; the one-electron transferred [$Fe^{II}_{LS}Fe^{III}_{LS}Co^{II}_{HS}Co^{III}_{LS}$] state and the 1:1 mixture of [$(Fe^{III}_{LS})_2(Co^{II}_{HS})_2$] and [$(Fe^{II}_{LS})_2(Co^{III}_{LS2})$] from the experimental results. To elucidate the possible states, total energies of these states: [$(Fe^{III}_{LS})_2(Co^{II}_{HS})_2$], [$(Fe^{II}_{LS})_2(Co^{III}_{LS})_2$] and [$Fe^{II}_{LS}Fe^{III}_{LS}Co^{II}_{HS}Co^{III}_{LS}$] are calculated using the **1-M** model structure. The results are summarized in Table 4. The most and the second most stable states are the PF and the PAF states of the [$Fe^{II}_{LS}Fe^{III}_{LS}Co^{II}_{HS}Co^{III}_{LS}$], and the third one is the ferromagnetic [$Fe^{III}_{LS2}Co^{II}_{HS2}$] state. On the other hand, the diamagnetic [$(Fe^{II}_{LS})_2(Co^{III}_{LS})_2$] state is unstable more than 1 eV in comparison with the PF and the PAF states. Therefore, an estimated energy of 1:1 mixture of [$(Fe^{III}_{LS})_2(Co^{II}_{HS})_2$] and [$(Fe^{II}_{LS})_2(Co^{III}_{LS})_2$] by

averaging their total energies is still unstable than the **1-M$_{PF}$** state about 0.75 eV. Based on the relative energies in the table, a population of each state at 298K is estimated by the Boltzmann distribution. The energy gap of 0.27 eV between **1-M$_{PF}$** and **1-M$_{F}$** is too large for a thermal excitation at 298K so that the population at the **1-M$_{F}$** and higher states is estimated to be almost zero. From those points of view, the electronic structure at the middle temperature is considered to be the one-electron transferred [$Fe^{II}_{LS}Fe^{III}_{LS}Co^{II}_{HS}Co^{III}_{LS}$] state. Nevertheless calculated result supports an asymmetric electronic structure, the X-ray geometry has C_2 symmetry. Hence, the experimental position of metal ions seems to be the average of Fe^{II} and Fe^{III} or Co^{II} and Co^{III} in the complex **1** in the crystal. So, if a structural asymmetry of the complex is considered, the [$Fe^{II}_{LS}Fe^{III}_{LS}Co^{II}_{HS}Co^{III}_{LS}$] i.e. PF and PAF states, will be more stabilized.

Table 4. Calculated total energies, relative energies and estimated populations at each state at 298K. $\langle S^2 \rangle$ values are also summarized in parentheses.

Models/States	Total Energy /atomic unit		Relative Energy / eV	Population / %
1-M$_{D}$	-9233.994914	(0.0000)	1.30	0.0
1-M$_{F}$	-9234.035569	(20.0573)	0.20	0.0
1-M$_{AF}$	-9234.032653	(8.0478)	0.27	0.0
1-M$_{PF}$	-9234.042748	(7.1891)	0.00	55.0
1-M$_{PAF}$	-9234.042558	(4.1876)	0.01	45.0
Average of **1-M$_{D}$** and **1-M$_{F}$**	-9234.015241		0.75	

3.4 One-electron excitation from Fe^{III} to Co^{II} *at the low temperature phase*

In order to elucidate the mechanism of the IVCT from Fe^{III} to Co^{II} in the diamagnetic [$(Fe^{II}_{LS})_2(Co^{III}_{LS})_2$] in low temperature phase, we carried out the TD-B3LYP calculation on the **1-L$_{D}$**. A simulated spectrum is depicted in Figure 5 and detailed data are summarized in Table S2 in Supplementary materials. There are many low excited states with zero or negligible oscillation strengths, so that 45 one-electron excited states are required to survey from the lowest excitation up to 700nm. As summarized in the

Table S2, obtained oscillation strengths are small and almost of all excitations concern with Fe → tp* MLCT. However, there are two significant peaks at 819 nm (ΔE = 1.51 eV) and 810 nm (ΔE = 1.53 eV). The dominant contributions of the peaks are excitations from Fe t_{2g} orbitals to Co e_g orbitals, clearly indicates that those two peaks concern with the Fe →Co IVCT. And many MLCT excitations around the IVCT peaks will contribute to their broadening. This result explains the very broad experimental peak of IVCT around 770nm.

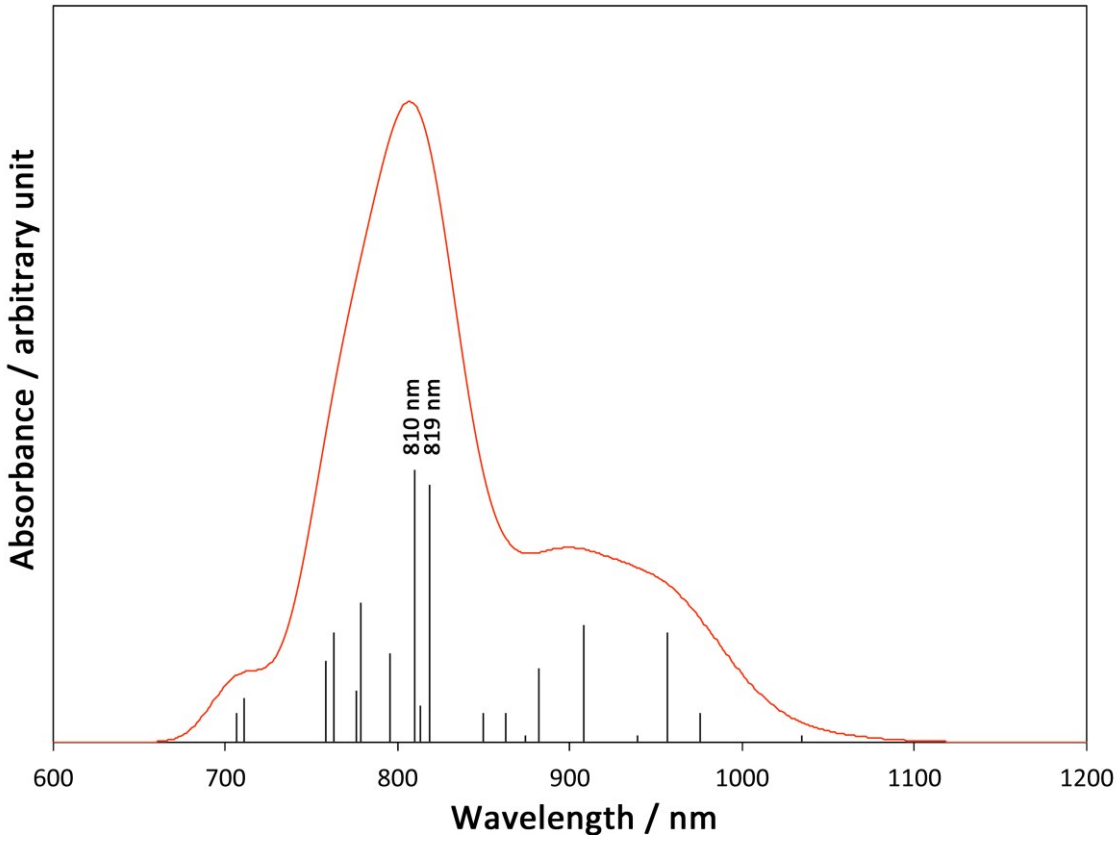

Figure 5. A simulated absorption spectrum based on the TD-B3LYP calculation. (Peak Width at Half Height is 0.05eV)

3. 5 Calculations of effective exchange coupling constant (J)

In above sections, we obtain the result that the F state is stable in comparison with the AF state. However there are other possible spin-coupling states in the open-shell $[(Fe^{III}_{LS})_2(Co^{II}_{HS})_2]$ state. To elucidate the stable spin-coupling state, the effective

exchange coupling constant (J) between Fe^{III} and Co^{II} is calculated by the energy gap between the F and the AF states of the open-shell state. The magnetic properties of the polynuclear metal complexes are often discussed by using Heisenberg Hamiltonian

$$H = -2\sum J_{ij}\hat{\boldsymbol{S}}_i \times \hat{\boldsymbol{S}}_j, \quad (1)$$

where J_{ij} is the orbital-averaged effective exchange integrals between the spin site i and j with total spin operators $\hat{\boldsymbol{S}}_i$ and $\hat{\boldsymbol{S}}_j$, respectively.[10, 15] Here, we only consider the isotropic spin term. As depicted in Figure 2 (a), there are three types interactions i.e. J, J' and J''. However, J' and J'' are considered to be small enough, so that we only consider the adjacent interaction J. A generalized scheme for calculations of J values is applied to the models. Based on the scheme, the J value between Fe^{III} and Co^{II} is obtained from

$$J = \frac{{}^{AF}E - {}^{F}E}{8\left\langle \hat{\boldsymbol{s}}_i \times \hat{\boldsymbol{s}}_j \right\rangle - {}^{AF}\left\langle \hat{\boldsymbol{s}}_i \times \hat{\boldsymbol{s}}_j \right\rangle}, \quad (2)$$

where ${}^{X}\left\langle \hat{\boldsymbol{s}}_i \times \hat{\boldsymbol{s}}_j \right\rangle$ is a spin correlation function of state X (X = F or AF). A detailed derivation of equation (2) is explained in Supplementary information.

All calculated J values summarized in Table 5 are positive, meaning that the magnetic interaction between Fe^{II} and Co^{III} is ferromagnetic. Based on the calculated J values of **1-H**, energy levels of five spin-coupling states in Figure S2 in Supplementary materials are estimated by solving spin Hamiltonian. Calculated results are summarized in Table S3 in Supplementary materials. As easily expected, calculated results indicate that the F and the AF states are the most stable and unstable states among the five spin-coupling states, respectively, and other states are intermediate. Similarly, the F state is more stable in comparison with the AF state in other temperature regions. This ferromagnetic interaction in the complex is consistent with other papers[14] and our previous report for the cyanide-bridged [Fe-Co] chain[12]. We also calculate the J value with Ising spin model, which consider only S_z component. The J values of the Ising model that are summarized in Table S3 in Supplementary materials thoroughly equal to those of the Heisenberg model within a computational convergence. The result shows that the spins on the metal sites are fully localized.

Table 5. Calculated *J* values of Heisenberg spin models.

Models	*J* value / cm^{-1}
1-L	22
1-M	53
1-H	11

4. Summary

In this study, we elucidate the detailed electronic and spin structures of the complex **1** that shows the CTIST. Calculated MOs of the full and the reduced model structures of the low temperature phase indicate that the shapes and orbital energy gaps of the both models are quite similar to each other, suggesting that the substituent groups contribute only to the structural stability but not to the properties of valence electrons. By comparison with total energies of the model structures, the ground states at LS and HT phases are the diamagnetic $[(Fe^{II}_{LS})_2(Co^{III}_{LS})_2]$ and the ferromagnetic $[(Fe^{III}_{LS})_2(Co^{II}_{HS})_2]$ states, respectively. At the intermediate phase, the one-electron transferred $[Fe^{II}_{LS}Fe^{III}_{LS}Co^{II}_{HS}Co^{III}_{LS}]$ state is preferable, while the total energy of the 1:1 mixture of $[(Fe^{III}_{LS})_2(Co^{II}_{HS})_2]$ and $[(Fe^{II}_{LS})_2(Co^{III}_{LS})_2]$ is too high for the thermal excitation. The calculated *J* values in the open-shell $[(Fe^{III}_{LS})_2(Co^{II}_{HS})_2]$ are positive, indicating that the ferromagnetic state is the most stable states among the other possible spin-coupling states. The significant two peaks around 800nm by TD-B3LYP calculation support that the experimental broad peak at 770nm is the IVCT band.

Acknowledgement

This work has been supported by Grant-in-Aid for Scientific Research (KAKENHI) (C) (No. 26410093) from Japan Society for the Promotion of Science (JSPS) and Grant-in-Aid for Scientific Research on Innovative Areas (“Coordination programming”, No. 24108721) from the Ministry of Education, Culture, Sports, Science and Technology (MEXT). We acknowledge Professor Hiroyuki Nojiri, the Institute for Materials Research (IMR), Tohoku University, for his significant discussions. And

this work was also performed under the Inter-University Cooperative Research Program of the Institute for Materials Research, Tohoku University (Proposal No. 14K0008, 15K0118). Finally, one of the authors (YK) acknowledges Toyota Physical and Chemical Research Institute Scholars.

Reference

1. W.-D. Griebler, D. Babel , *Naturforsch* 1982, *37b*, 832.
2. V. Gadet, T. Mallah, I. Castro, M. Verdaguer, *J. Am. Chem. Soc.*, 1992, *114*, 9214.
3. T. Mallah, S. Thiébaut, M. Verdaguer, P. Veillet, *Science*, 1993, *262*, 1554
4. S. Ferlay, T. Mallah, R. Ouahès, P. Veillet, M. Verdaguer, *Nature*, 1995, *378*, 701
5. O. Sato, T. Iyoda, A. Fujishima, K. Hashimoto, *Science*, 1996, 272, 704.
6. (a) M. Nihei, Y. Sekine, N. Suganami, H. Oshio, *Chem. Lett*., 2010, 39, 978; (b) M. Nihei, Y. Sekine, N. Suganami, K. Nakazawa, A. Nakao, H. Nakao, Y. Murakami, H. Oshio, *J. Am. Chem. Soc*., 2011, 133, 3592; (c) Y. Sekine, M. Nihei, R. Kumai, H. Nakao, Y. Murakami, H. Oshio, *Chem. Commun.* 2014, 50, 4050. (d) Y. Sekine, M. Nihei, R. Kumai, H. Nakao, Y. Murakami, H. Oshio, *Inorg. Chem. Front.* 2014, 1, 540; (e) Y. Sekine, M. Nihei, H. Oshio, *Chem. Lett.*, 2014, 43, 1029.
7. (a) P. Gütlich, A. Hauser, H. Spiering, *Angew. Chem. Int. Ed.*, 1994, 33, 2024. (b) N. Shimamoto, S. Ohkoshi, O. Sato, K. Hashimoto, *Inorg. Chem.*, 2002, 41, 678 (c) A.B. Gaspar, V. Ksenofontov, M. Seredyuk, P. Gütlich, *Coord. Chem. Rev.* 2005, 249, 2661.
8. (a) W.E. Bushmann, J. Ensling, P. Gütlich, J.S. Miller, *Chem.Eur. J*. 1999, 5, 3019; (b) W.R. Entley, G.S. Girolami, *Inorg. Chem.* 1994, 33, 5165; (c) J. Larionova, R. Clérac, J. Sanchiz, O. Kahn, S. Golhen, L. Ouahab, *J. Am. Chem. Soc.* 1998, 120, 13088; (d) E. Coronado, M.C. Giménez-López, G. Levchenko, F.M. Romero, V. Garcia-Baonza, A. Milner, M. Paz-Pastemak, *J. Am. Chem. Soc.* 2005, 127, 4580;(e) W. Kosaka, K. Nomura, K. Hashimoto, S. Ohkoshi, *J.Am. Chem. Soc.* 2005, 127, 8590. (f) S. Ohkoshi, H. Tokoro, T. Matsuda, H. Takahashi, H. Irie, K. Hashimoto, *Angew. Chem.Int. Ed.* 2007, 46, 3238
9. (a) O. Sato, J. Tao, Y.-Z. Zhang, *Angew. Chem. Int. Ed.*, 2007, 46, 2152. (b) A. Bousseksou, G. Molnar, L. Salmon, W. Nicolazzi, *Chem. Soc. Rev.*, 2011, 40, 3313.

(c) A. Bleuzen, V. Marvaud, C. Mathoniere, B. Sieklucka, M. Verdaguer, *Inorg. Chem.* 2009, 48, 3453. (d) J.-D. Cafun, J. Lejeune, J.-P. Itié, F. Baudelet, A. Bleuzen, *J. Phys. Chem.* C, 2013, 117, 19645.

10. O. Kahn, *Molecular Magnetism*, VCH, New York, 1993.
11. (a) C.P. Berlinguette, A. Dragulescu-Andrasi, A. Sieber, J.R. Galán-Mascarós, H-U. Güdel, C. Achim, K.R. Dunbar, *J. Am. Chem. Soc.*, 2004, *126*, 6222. (b) D. Li, R. Clérac, O. Roubeau, E. Harté, C. Mathonière, R.L. Bris, S.M. Holmes, *J. Am. Chem. Soc.*, 2008, 130, 252. (c) Y. Zhang, D. Li, R. Clérac, M. Kalisz, C. Mathonière, S.M. Holmes, *Angew. Chem. Int. Ed.* 2010, 49, 3752. (d) D. Li, R. Clérac, O. Roubeau, E. Harté, C. Mathonière, R. Le Bris, S. M. Holmes, *J. Am. Chem. Soc.* 2008, 130, 252. (e) G.N. Newton, M. Nihei, H. Oshio, Eur. J. *Inorg. Chem.*, 2011, 2011, 3031. (f) A. Mondal, Y. Li, M. Seuleiman, M. Julve, L. Toupet, M.B-L Cointe, Lescouëzec, R. *J. Am. Chem. Soc.* 2013, 135,1653.
12. (a) N. Hoshino, F. Iijima, G. N. Newton, N. Yoshida, T. Shiga, H. Nojiri, A. Nakao, R. Kumai, Y. Murakami, H. Oshio, *Nat. Chem.* 2012, 4, 921. (c) M.L. Baker, Y. Kitagawa, T. Nakamura, K. Tazoe, Y. Narumi, Y. Kotani, F. Iijima, G. N Newton, M. Okumura, H. Oshio, H. Nojiri, *Inorg. Chem.*, **2013**, *52*, 13956
13. (a) M. Nihei, Y. Okamoto, Y. Sekine, N. Hoshino, T. Shiga, I. P.-C. Liu, H. Oshio, *Angew. Chem., Int. Ed.* 2012, 51, 6361. (b) K. Mitsumoto, E. Oshiro, H. Nishikawa, T. Shiga, Y. Yamamura, K. Saito, H. Oshio, *Chem. Eur. J.* 2011, 17, 9612. (c) H. Oshio, N. Hoshino, T. Ito, M. Nakano, *J. Am. Chem. Soc.*, 2004, 126, 8805.
14. (a) M. Nishino, Y. Yoshioka, K. Yamaguchi, *Chem Phys Lett.*, 297, 1998, 51.; (b) K. Yoshizawa, F. Mohri, G. Nuspl, T. Yamabe, *J. Phys. Chem.* B 1998, 102, 5432.; (c) M. Atanasov, P. Comba, C.A. Daul, *J. Phys. Chem A*, 2006, 110, 13332.; (d) L. Kabalan, S.F. Matar, C. Desplanches, J.F. Létard, M. Zakhour, *Chem. Phys.* 2008, 352, 85.
15. (a) A.P. Ginsberg, J. Am. Chem. Soc. 1980, 102, 111. (b) L. Noodleman, *J. Chem. Phys.* 1981, 74, 5737. (c) A. Bencini, F. Totti, C.A. Daul, K. Doclo, P. Fantucci, V.Barone, *Inorg. Chem.* 1997, 36, 5022. (d) M. Deumal, J.J. Novoa, M.J. Bearpark, P. Celani, M. Olivucci, M.A. Robb, *J. Phys. Chem.* A, 1998, 102, 8404. (e) R. Caballol, O. Castell, F. Illas, I. de P. R. Moreira J. P. Malrieu, *J. Phys. Chem.* A, 1997, 101, 7860, (f) E. Ruiz, J. Cano, S. Alvarez, P. Alemany, *J. Comp. Chem.*

1999, 20, 1391. (g) S. Vela, M. Deumal, M. Shiga, J. J. Novoa, J. Ribas-Arino, *Chem. Sci.*, 2015, 6, 2371.

16. (a) K. Yamaguchi, in: R. Carbo, M. Klobukowski (Eds.), Self-Consistent Field Theory and Applications, Elsevier, Amsterdam, 1990, p. 727., (b) S. Yamanaka, T. Kawakami, H. Nagao, K. Yamaguchi, *Chem. Phys. Lett.* 231 (1994) 25. (c) T. Soda, Y. Kitagawa, T. Onishi, Y. Takano, Y. Shigeta, H. Nagao, Y. Yoshioka, K. Yamaguchi, *Chem. Phys. Lett.* 2000, **319**, 223; (d) M. Shoji, K. Koizumi, Y. Kitagawa, T. Kawakami, S. Yamanaka, M. Okumura, K. Yamaguchi, *Chem. Phys Lett.* 2006, 432, 343; (e) Y. Kitagawa, T. Matsui, N. Yasuda, H. Hatake, T. Kawakami, S. Yamanaka, M. Nihei, M. Okumura, H. Oshio, K. Yamaguchi, *Polyhedron*, 2013, 66, 97.
17. (a) Low temperature phase measured at 100K (CCDC ID: KAFXAS), (b) Intermediate phase measured at 298K (CCDC ID: KAFXAS01), (c) high temperature phase measured at 330K (CCDC ID: KAFXAS02).
18. Gaussian 09, Revision C.01, M. J. Frisch, G. W. Trucks, H. B. Schlegel, G. E. Scuseria, M. A. Robb, J. R. Cheeseman, G. Scalmani, V. Barone, B. Mennucci, G. A. Petersson, H. Nakatsuji, M. Caricato, X. Li, H. P. Hratchian, A. F. Izmaylov, J. Bloino, G. Zheng, J. L. Sonnenberg, M. Hada, M. Ehara, K. Toyota, R. Fukuda, J. Hasegawa, M. Ishida, T. Nakajima, Y. Honda, O. Kitao, H. Nakai, T. Vreven, J. A. Montgomery, Jr., J. E. Peralta, F. Ogliaro, M. Bearpark, J. J. Heyd, E. Brothers, K. N. Kudin, V. N. Staroverov, R. Kobayashi, J. Normand, K. Raghavachari, A. Rendell, J. C. Burant, S. S. Iyengar, J. Tomasi, M. Cossi, N. Rega, J. M. Millam, M. Klene, J. E. Knox, J. B. Cross, V. Bakken, C. Adamo, J. Jaramillo, R. Gomperts, R. E. Stratmann, O. Yazyev, A. J. Austin, R. Cammi, C. Pomelli, J. W. Ochterski, R. L. Martin, K. Morokuma, V. G. Zakrzewski, G. A. Voth, P. Salvador, J. J. Dannenberg, S. Dapprich, A. D. Daniels, Ö. Farkas, J. B. Foresman, J. V. Ortiz, J. Cioslowski, and D. J. Fox, Gaussian, Inc., Wallingford CT, 2009.
19. (a) H. Fukutome, *Prog. Theoret. Phys.* 1972, 47, 1156. (b) A. Szabo, N.S Ostlund, Modern Quantum Chemistry, Dover, New York, NY, 1996, p. 205.